Probing the Electronic Structure of $[B_{10}H_{10}]^{2-}$ Dianion Encapsulated by an Octamethylcalix[4]pyrrole Molecule

Wenjin Cao, Jonas Warneke, and Xue-Bin Wang*

ABSTRACT: Despite being an important *closo*-borate in condensed phase boron chemistry, isolated $[B_{10}H_{10}]^{2-}$ is electronically unstable and has never been detected in the gas phase. Herein, we report a successful capture of this fleeting species through binding with an octamethylcalix[4]pyrrole (omC4P) molecule to form a stable gaseous omC4P·$[B_{10}H_{10}]^{2-}$ complex and its characterizations utilizing negative ion photoelectron spectroscopy (NIPES). The recorded NIPE spectrum, contributed by both omC4P and $[B_{10}H_{10}]^{2-}$, is deconvoluted by subtracting the omC4P contribution to yield a $[B_{10}H_{10}]^{2-}$ spectrum. The obtained $[B_{10}H_{10}]^{2-}$ spectrum consists of four major bands spanning the electron binding energy (EBE) range from 1 to 5 eV, with the EBE gaps matching excellently with the energy intervals of computed high-lying occupied molecular orbitals of the $[B_{10}H_{10}]^{2-}$ dianion. This study showcases a generic method to utilize omC4P to capture unstable multiply charged anions in the gas phase for experimental determination of their electronic structures.

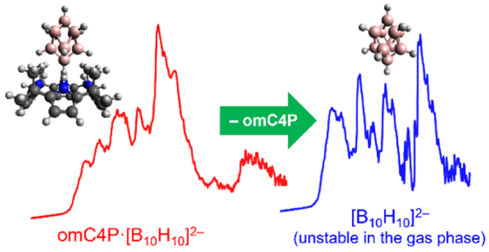

1. INTRODUCTION

closo-Boranes are textbook boron compounds that have received extensive research interest for decades.[1] Since the successful synthesis of the first icosahedral $[B_{12}H_{12}]^{2-}$ anion back in 1960,[2] polyhedral borate anions of general formula $[B_nX_n]^{2-}$ and their analogs are not only subject to continuous fundamental research[3−7] but also have been widely explored in applications[8] like boron-based neutron capture therapy of cancer and solid-state batteries.[8−15] Following $[B_{12}H_{12}]^{2-}$, the second most important representative of this anion class is the $[B_{10}H_{10}]^{2-}$ dianion (*closo*-decaborate),[16] whose salts are easily accessible. It is well-known that there are remarkable differences in the fundamental chemical and physical properties of *closo*-dodecaborates that are dependent on cluster size n and substituent X.[17−20] These differences also influence their interaction with other molecules and ions substantially, which can be important, for example, in the context of medical applications: deca- and dodecaborate (n = 10, 12) derivatives have been shown to differ in their metabolic pathways.[21,22] Precisely adjusting interactions with other molecules for medical and material science applications may be achieved only if the chemical and physical properties of the ions are understood at the fundamental molecular level.

In the recent years, negative ion photoelectron spectroscopy (NIPES)[23] has been employed to investigate polyhedron *closo*-borate dianions,[24] with a general formula of $[B_nX_n]^{2-}$ (X = H, CN, or a halogen atom, n = 6, 10−12) unraveling their intrinsic electronic structures, bonding properties, and molecular orbitals (MO).[18,19,25−27] In addition, NIPES combined with tagging-based infrared photodissociation spectroscopy, collision-induced dissociation mass spectrometry, and computational chemistry has been utilized to explore the effects of specific functional groups on the electronic stabilities and chemical reactivities of *closo*-borate anions.[28] Through these studies, NIPES has been demonstrated as a powerful tool to investigate gaseous molecular properties of isolated *closo*-borate dianions without interference from solvent molecules or counterions.

One major challenge in characterizing some of these dianions utilizing NIPES is the electronic instability arising from strong Coulomb repulsion between the two excess electrons,[29,30] which is especially pronounced for the *closo*-hydroborates (X = H) without strong electron-withdrawing groups to stabilize the dianions. Though perhalogenated *closo*-borates become stable starting with the boron cage size of n = 6,[24] only 12−vertexed $[B_{12}H_{12}]^{2-}$ was identified as a stable *closo*-hydroborate dianion in the gas phase.[25,31] This parallels with a couple of theoretical studies that predict electronic instabilities for smaller $[B_nH_n]^{2-}$ dianions.[31−34] Consequently, intrinsic electronic structural information for $[B_nH_n]^{2-}$ dianions with n smaller than 12 has not been spectroscopically probed because their isolation in the gas phase is not possible. Our previous NIPES work illustrated substantially different spectral patterns in electronic states for the 10- or 11-vertexed

perhalogenated *closo*-borate dianions compared to their corresponding 12-vertexed ones.[18] In parallel, distinct spectral patterns and electronic structure information are expected for different sizes of $[B_nH_n]^{2-}$ dianions, which have not been explored to date for $n < 12$.

closo-Decahydroborate, $[B_{10}H_{10}]^{2-}$ is among the most investigated hydroborates in the chemistry of the condensed phases.[16,35−37] It was predicted to be the second most stable $[B_nH_n]^{2-}$ dianion only after $[B_{12}H_{12}]^{2-}$.[32] Nevertheless, isolated $[B_{10}H_{10}]^{2-}$ is electronically unstable with respect to the second electron autodetachment,[32] and substantial stabilization is thus required to enable it to be detected in the gas phase. Solvent molecules or counterions are known to afford such stabilizations when binding to the dianion and are candidates to be considered.[38] Traditional solvent molecules like H_2O typically afford modest stabilization toward an anion. Usually, multiple solvent molecules are required to prevent electron detachment from an intrinsically unstable dianion.[39] For superchaotropic *closo*-borate dianions, the stabilization from H_2O molecules is quite limited.[40,41] On the other hand, the stabilization arising from a counterion is very strong and may shift lower-lying molecular orbitals (MOs) out of the measurable range.[18] A moderate stabilization effect is often afforded by organic host molecules known to effectively encapsulate *closo*-borate dianions.[42−47] Furthermore, the stabilization from a large organic host molecule is usually more symmetric compared to that afforded by a solvent molecule or a counterion, thus avoiding the disturbance of the electronic structure of the ion under investigation. Such disturbance has become obvious in microsolvated $[B_{12}I_{12}]^{2-}$,[41] as well as the $[KB_{12}H_{12}]^-$ ion pair (Figure S1), both exhibiting significantly broadened spectral profiles compared to the isolated species. Although encapsulation with a symmetric host molecule minimizes these disturbances, other issues may hinder a straightforward determination of the intrinsic electronic structure using this approach: due to energetically close-lying MOs of host molecule and guest ion, the measured NIPE spectrum of the host−guest complex could exhibit spectral features arising from overlapping bands of the individual host and guest component. This has been seen from NIPE spectra of various cyclodextrin-*closo*-dodecaborate complexes.[45,46] To characterize the $[B_{10}H_{10}]^{2-}$ dianion using a host molecule, an effective approach to distinguish between these two components is necessary.

Very recently, we carried out an NIPES study on a series of host−guest complexes of various halides or pseudohalides encapsulated in an octamethylcalix[4]pyrrole (omC4P) molecule, illustrating that the observed host−guest spectra can be effectively deconvoluted into contributions from omC4P host and guest ions.[48] This is based on the fact that all spectral bands in the NIPE spectrum of omC4P·F^- solely originate from the ionization of the host omC4P within the 0−7.8 eV range. Although the exact spectral band position on the binding energy scale is dependent on the encapsulated anion, the shape and relative band positions are almost independent, thus allowing us to deduce the host contribution from the recorded complex spectrum that, in turn, enables the guest anion spectral bands to be obtained, which retains the spectral feature of the isolated anion but just blue shifts in electron binding energy (EBE). As a common organic host molecule with multiple hydrogen bond donors,[49,50] omC4P is, therefore, an ideal molecule to encapsulate $[B_{10}H_{10}]^{2-}$ so that the complex could be stabilized in the gas phase and its electronic structure could then be determined experimentally. In this work, we employ this strategy to record the NIPE spectrum of the omC4P·$[B_{10}H_{10}]^{2-}$ complex and, in turn, determine the electronic structure of isolated $[B_{10}H_{10}]^{2-}$, which is not directly measurable. Since the spectral feature of the omC4P host is known,[48] the NIPE spectrum of $[B_{10}H_{10}]^{2-}$ can then be deducted. The extracted $[B_{10}H_{10}]^{2-}$ spectrum matches excellently with the accompanying theoretical predictions and provides the first experimental electronic structure characterization for this important dianion. Comparing the spectrum of $[B_{10}H_{10}]^{2-}$ with that of $[B_{12}H_{12}]^{2-}$ reveals substantial differences between the two and illustrates the sensitive size-dependence of the electronic structure of hydroborates.

2. METHODS

2.1. Experimental Methods. Negative ion photoelectron spectroscopy (NIPES) experiments were carried out using a magnetic-bottle time-of-flight (TOF) photoelectron spectrometer combined with an electrospray ionization (ESI) source and a temperature-controlled cryogenic ion trap, as described elsewhere.[23] The omC4P·SO_4^{2-}, omC4P·$[B_{10}H_{10}]^{2-}$, and omC4P·$[B_{12}X_{12}]^{2-}$ (X = H, F − I) complex dianions were generated by electrospraying ∼1 mM solutions of omC4P and *n*-tertbutyl ammonium salts of corresponding dianions dissolved in acetonitrile. The resulting anions were transported by a radio frequency quadrupole ion guide and first detected by a quadrupole mass spectrometer, during which the ESI conditions were optimized to ensure stable and intense ion cluster beams. A 90° bender was used to direct the anions into the cryogenic 3D ion trap, where they were accumulated for 20−100 ms and cooled by collisions with a cold buffer gas (20% H_2 balanced in He) to 20 K before being pulsed out into the extraction zone of the TOF mass spectrometer for mass analysis at a repetition rate of 10 Hz. Desired complex anions were mass-selected and decelerated before being photodetached by a probe laser beam in the interaction zone of the magnetic-bottle photoelectron analyzer. A 157 nm (7.867 eV, Lambda Physik CompexPro F_2) laser beam, operated at a 20 Hz repetition rate with the anion beam shut off on alternating laser shots to afford shot-to-shot background subtraction, was used for photodetachment. The resulting photoelectrons were collected at nearly 100% efficiency in the magnetic bottle and analyzed with a 5.2 m-long electron flight tube. Recorded flight times were converted into kinetic energies calibrated using the known spectra of I^-/$OsCl_6^{2-}$.[51,52] The electron binding energy spectra were obtained by subtracting the electron kinetic energies from the detachment photon energy with an electron energy resolution ($\Delta E/E$) of about 2% (i.e., ∼20 meV for 1 eV kinetic energy electrons).

2.2. Computational Details. Geometries of various dianions and complexes with the omC4P molecule were initially optimized by density functional theory (DFT) using M06-2X[53] with Grimme's D3 dispersion correction (denoted M06-2X-D3),[54] coupled with the def2-SVP basis set.[55] Frequency analyses were carried out at the same level of theory to ensure that located structures were true local minima. These preliminary structures were subsequently optimized with the maug-cc-pVTZ[56,57] basis set (maug-cc-pVTZ-PP[58] for Br and I). Single point energies of singly charged complexes at the optimized dianionic geometries were also calculated at the same level of theory to yield computational VDEs for each of the complexes. In addition, the domain-based local pair natural

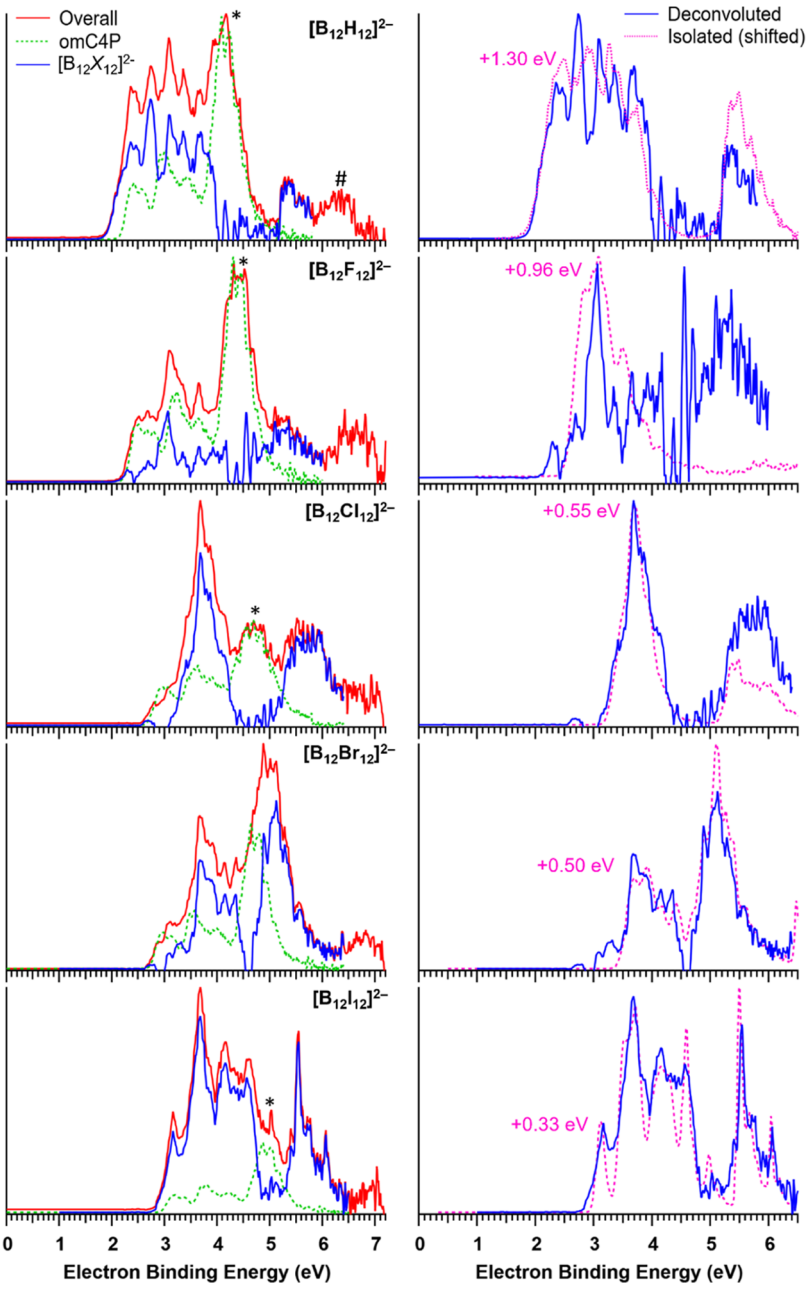

Figure 1. Left panel: Deconvolutions of NIPE spectra of omC4P·$[B_{12}X_{12}]^{2-}$ (X = H, F, Cl, Br, and I, red traces) into two components contributed by omC4P (green dotted lines) and guest ions (blue traces); right panel: comparisons of deconvoluted spectra for $[B_{12}X_{12}]^{2-}$ (X = H, F, Cl, Br, and I, blue traces) and those measured for isolated dianions (pink dotted lines). The outstanding features of the omC4P·$[B_{12}X_{12}]^{2-}$ spectra to locate omC4P contributions are marked with "*". The spectra of isolated $[B_{12}X_{12}]^{2-}$ are adapted with permission from refs 26 and 41 (copyright 2017 and 2022 American Chemical Society) and are shifted to overlap with deconvoluted ones. The VDE shifts are given in pink numbers. Feature # likely originates from omC4P and is suggested from the computed MO levels (Figure S2).

orbital coupled cluster theory (DLPNO−CCSD(T))[59] has been utilized using the same basis set to refine the VDEs for smaller dianions and to validate the M06-2X-D3 values. Basis set superposition error (BSSE)-[60,61] corrected dissociation energies (D_es) were also computed at the M06-2X-D3 level of theory for dianionic complexes without reoptimizing fragment geometries. The resolution-of-the-identity (RI) approximation for Coulomb- and exchange-type integrals (RIJK)[62] was used to speed up the calculation with matching auxiliary basis sets. All of these quantum chemical calculations were carried out with the ORCA 5.0.4 package.[63,64] In addition, the atomic charges of the $[B_{10}H_{10}]^{2-}$ dianion were computed with charges from electrostatic potentials using a grid-based (CHELPG)[65] method implemented in Multiwfn.[66]

3. RESULTS AND DISCUSSION

3.1. Deconvolutions of omC4P·$[B_{12}X_{12}]^{2-}$ Complexes.

The protocol is first validated through deconvoluting a series of NIPE spectra of omC4P·$[B_{12}X_{12}]^{2-}$ (X = H, F − I) complexes (Figure 1). To obtain deconvoluted $[B_{12}X_{12}]^{2-}$ spectra, we first identified the features arising from the omC4P host with the assistance of M06-2X-D3 calculations that predict relative energies of MOs dominated by omC4P or $[B_{12}X_{12}]^{2-}$ (Figure S2). For X = F − Br, the HOMOs are

Table 1. Vertical Detachment Energies (VDEs) of Sulfate, *closo*-Deca- or Dodecaborates upon Encapsulated by omC4P, and as Isolated Dianions and Their Differences (ΔVDEs), Apparent Vertical Ionization Energies (VIEs) of omC4P from Spectral Deconvolution and Their Differences to that of Isolated omC4P Molecule (ΔVIEs), as well as Calculated (calc.) BSSE-Corrected Dissociation Energies (D_es) at the M06-2X-D3 Level of Theory

	VDE of guest dianions			VIE of omC4P		
	in complex	isolated[a]	ΔVDE	in complex	ΔVIE[e]	calc. D_e
SO_4^{2-}	2.50	n/a (−1.09;−0.87)	3.59[d]	1.42	−4.93	5.28
$[B_{10}H_{10}]^{2-}$	1.58	n/a (−0.17;−0.14)	1.75[d]	2.04	−4.31	3.20
$[B_{12}H_{12}]^{2-}$	2.40	1.15[b] (1.16[b];1.32)	1.25	2.42	−3.93	2.40
$[B_{12}F_{12}]^{2-}$	3.06	1.90[c] (n/a;2.37)	1.16	2.50	−3.85	1.96
$[B_{12}Cl_{12}]^{2-}$	3.50	2.95[c] (n/a;3.27)	0.55	2.95	−3.40	1.57
$[B_{12}Br_{12}]^{2-}$	3.70	3.20[c] (n/a;3.37)	0.50	2.97	−3.38	1.55
$[B_{12}I_{12}]^{2-}$	3.16	2.80[c] (n/a;3.37)	0.36	3.18	−3.17	1.48

[a]Experimental VDEs (available or not available n/a). The values in parentheses are calc. VDEs at the CCSD(T) and M06-2X levels of theory. [b]From ref 25. [c]From ref 26. [d]Compared to the CCSD(T) computed values when experimental VDEs are not available. [e]Compared to estimated isolated omC4P molecule VIE of 6.35 eV from ref 48.

clearly dominated by omC4P, and therefore, the lowest EBE bands are predominantly from the host. In addition, the strongest band feature arising from the omC4P host molecule (marked with an "*") is also a good reference in most complexes except for omC4P·$[B_{12}Br_{12}]^{2-}$, which is especially useful for omC4P·$[B_{12}H_{12}]^{2-}$ or omC4P·$[B_{12}I_{12}]^{2-}$, whose HOMO is dominated by the guest dianion or unclear. Subsequently, the previously recorded omC4P·F^- spectrum, which is solely determined by the electronic structure of the omC4P host molecule, is shifted in EBE to ensure the strongest band aligned with the outstanding feature "*" (for omC4P·$[B_{12}H_{12}]^{2-}$ or omC4P·$[B_{12}I_{12}]^{2-}$) or the rising edge is overlapping with the observed spectrum (for X = F − Br). The deconvoluted spectra for $[B_{12}X_{12}]^{2-}$ are then obtained by subtracting them from the spectra of the complexes. It is worth noting that the interactions between these doubly charged guest anions and the omC4P host are stronger compared to the singly charged guests previously studied,[48] thus shifting spectral features arising from ionizing omC4P further to the red, exhibiting large ΔVIE values (difference between apparent vertical ionization energy of omC4P determined from each deconvoluted omC4P spectrum and that of isolated omC4P molecule, which is estimated as 6.35 eV in a previous study[48]) as shown in Table 1. Due to the absence of a good reference for high EBE features, the deconvolution could not perfectly cover the spectral range beyond 6 eV. For example, the deconvolution for omC4P·$[B_{12}H_{12}]^{2-}$ is carried out up to ∼5.8 eV, with an extra band feature (labeled with a "#" in Figure 1) that likely originates from omC4P as suggested from the computed MO levels (Figure S2). As shown in Figure 1, the deconvoluted spectra contributed from the $[B_{12}X_{12}]^{2-}$ moieties in the complexes nicely match the spectra of isolated $[B_{12}X_{12}]^{2-}$, except for $[B_{12}F_{12}]^{2-}$. The quality of the deconvoluted spectrum suffers from extremely small photodetachment cross section compared to that of omC4P and therefore exhibits a poorly defined spectral pattern with a low signal-to-noise ratio. Nevertheless, the EBE of its major band feature can still be determined. No spectral broadening as shown in the case of $[KB_{12}H_{12}]^-$ (Figure S1) or $[B_{12}I_{12}]^{2-}\cdot nH_2O$ complexes[41] is present here. Such comparisons demonstrate that binding with an omC4P molecule could effectively retain the spectral pattern of the corresponding isolated guest species.

It is expected that the host−guest dissociation energy (D_e) correlates with the electronic stabilization of the guest anion. Therefore, an increase of the ΔVDE value (VDE determined from deconvoluted guest ion spectrum—VDE measured for the isolated ion) should result in a higher D_e[38,45,46] while, in the meantime, leading to a more negative ΔVIE value. In general, a systematic descending trend in ΔVDE and an ascending trend in ΔVIE are observed for X = H, F−I, qualitatively agreeing with the trend in calculated D_es for these complexes (Table 1). In omC4P·$[B_{12}X_{12}]^{2-}$ (X = H, F), one omC4P molecule affords a ΔVDE of 1.25 and 1.16 eV, equivalent to those afforded by 5 and 6 water molecules, respectively.[41] In these two complexes, the omC4P adopts the cone configuration, in which all four N−H bonds point at the same focal point on its C_4 molecular axis but slightly tilt to facilitate multiple interactions between borate ligands X and the host molecule (see the optimized geometry of omC4P·$[B_{12}H_{12}]^{2-}$ in Figure 2c). For larger $[B_{12}X_{12}]^{2-}$ (X = Cl − I) ions, the electronic stabilizations affected by omC4P are smaller, and ΔVDE values were found in the range of 0.55−0.36 eV (Table 1). Nevertheless, the ΔVDE = 0.36 eV for $B_{12}I_{12}^{2-}$ is still equivalent to that provided by 3 water molecules.[41] For X = Cl−I, omC4P no longer possesses a cone-shaped conformation. Instead, one of the four N−H bonds points toward the opposite direction (see the optimized omC4P·$[B_{12}Cl_{12}]^{2-}$ structure in Figure 2d). This magnitude of stabilization offered by the host omC4P is found adequate to even stabilize unstable dianions, e.g., sulfate,[39] affording a stabilization approximately equivalent to that by 7 H_2O molecules (Figure S3).

3.2. Deconvolutions of omC4P·$[B_{10}H_{10}]^{2-}$ Complex.

The *closo*-decaborate dianion $[B_{10}H_{10}]^{2-}$ adopts a D_{4d} point group with two types of symmetry equivalent B atoms: the two axial B atoms along the C_4 axis with an inner cluster connectivity of 4 and eight equatorial ones with an inner cluster connectivity of 5 (Figure 2).[18] Isolated $[B_{10}H_{10}]^{2-}$ is predicted to be electronically unstable with a negative VDE (Table 1) and has never been detected in the gas phase. Upon binding with omC4P, a stable omC4P·$[B_{10}H_{10}]^{2-}$ complex, in which the geometric parameters of the $[B_{10}H_{10}]^{2-}$ dianion are largely retained (Table S1), is detected, allowing to obtain a NIPE spectrum of the complex. As shown in Figure 3a, the NIPE spectrum of omC4P·$[B_{10}H_{10}]^{2-}$ consists of six major bands **I**−**VI** ranging from 1 to 7 eV, with the lowest band **I** peaked at 1.58 eV. M06-2X-D3/maug-cc-pVTZ optimization exhibits an axial B−H bond interacting with the N−H bonds from omC4P to form four B−H···H−N dihydrogen bonds

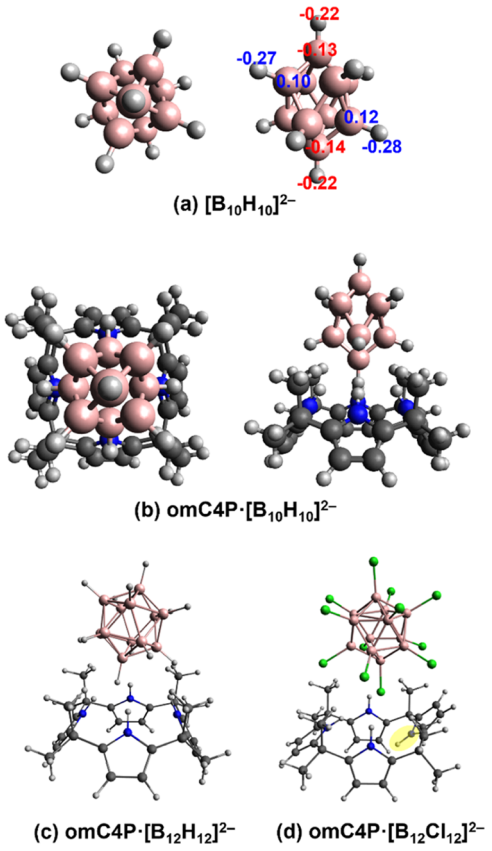

Figure 2. Top (left) and side (right) views of optimized structures for $[B_{10}H_{10}]^{2-}$ (a) and omC4P·$[B_{10}H_{10}]^{2-}$ (b) with respect to the C_4 molecular axis, as well as side views of optimized omC4P·$[B_{12}H_{12}]^{2-}$ (c) and omC4P·$[B_{12}Cl_{12}]^{2-}$ (d). The calculated atomic charges based on charges from electrostatic potentials using a grid-based method (CHELPG) for symmetry unique B and H atoms in $[B_{10}H_{10}]^{2-}$ are listed with red and blue numbers for axial and equatorial atoms, respectively. The balls representing atoms in omC4P·$[B_{12}H_{12}]^{2-}$ and omC4P·$[B_{12}Cl_{12}]^{2-}$ are intentionally shrunk for a clearer view. The N–H that points toward the opposite direction in omC4P·$[B_{12}Cl_{12}]^{2-}$ is highlighted in yellow.

(DHBs), with the C_4 axes of both moieties aligned, leading to a C_{4v} symmetry for the complex (Figure 2). The DHB distance between B–H and H–N is predicted to be 1.97 Å. The HOMOs of omC4P·$[B_{10}H_{10}]^{2-}$ are a set of doubly degenerate MOs dominated by the $[B_{10}H_{10}]^{2-}$ dianion (Figure 3a). The $[B_{10}H_{10}]^{2-}$ moiety also has significant contributions to bands **III**, **IV**, **V**, and **VI**. Combining the computed energetically high-lying MOs from both $[B_{10}H_{10}]^{2-}$ and omC4P, a simulated DOS spectrum is generated and agrees excellently with the experiment, except for the high EBE bands (>5 eV), where their intensity is expected to be suppressed by the repulsive Coulomb barrier (RCB)[26,29] in the experiments and, in fact, a tunneling signal through RCB.[67]

Deconvolution of this complex spectrum by aligning the strongest band in the omC4P reference spectrum with the band maximum of **V** in the observed spectrum followed by subtracting the omC4P contribution yields a blue-shifted $[B_{10}H_{10}]^{2-}$ spectrum in an EBE range from 1 to 5 eV that consists of four major bands **a**, **b**, **c**, and **d**, at 1.58, 2.40, 3.15, and 4.18 eV, respectively (Figure 3). In addition, there is a feature (marked with an "*") at an even higher EBE of 5.15 eV but is much weaker in intensity compared to other bands. The lowest EBE band **I** in the complex spectrum turns out to come from the $[B_{10}H_{10}]^{2-}$ moiety. Comparing the EBE of band **a** (1.58 eV) to the CCSD(T) computed VDE (−0.17 eV) of isolated $[B_{10}H_{10}]^{2-}$ leads to an estimated electronic stabilization of 1.75 eV offered by binding to omC4P, which is significant but still appreciably smaller than the calculated D_e of 3.20 eV. The deconvoluted spectrum contributed from the $[B_{10}H_{10}]^{2-}$ moiety is expected to resemble the isolated dianion's spectrum in all aspects except that the whole spectrum is blue-shifted by 1.75 eV (as demonstrated in omC4P·$[B_{12}X_{12}]^{2-}$, Figure 1). Therefore, the spectral pattern of the deconvoluted spectrum does reflect the relative energies of high-lying MOs of the $[B_{10}H_{10}]^{2-}$ dianion, serving as an effective way to probe the electronic structure of otherwise undetectable dianions (Figure 3c). Our computations indeed show that the high-lying MOs of the isolated $[B_{10}H_{10}]^{2-}$ dianion (Figure 4) share a pattern nearly identical to those in omC4P·$[B_{10}H_{10}]^{2-}$ that are dominated by the $[B_{10}H_{10}]^{2-}$ moiety (Figures 3a,c and S4 for a direct comparison). The HOMO of $[B_{10}H_{10}]^{2-}$ is doubly degenerate and dominated by boron atomic orbitals, followed by another two sets of doubly degenerate MOs (HOMO−1, HOMO−2) with slightly more contributions from H atomic orbitals (Figure 4). Eight deeper MOs are also located within the detection photon energy limit (Figure 3c). Based on computed relative energies of high-lying MO levels, the simulated DOS spectrum of isolated $[B_{10}H_{10}]^{2-}$ has reached an excellent agreement with that deconvoluted from the omC4P·$[B_{10}H_{10}]^{2-}$ spectrum in the EBE range up to ∼5 eV, whereas the higher EBE features exhibit weaker intensity or are completely missing due to the RCB, which provides a barrier for electron detachment from multiply charged anions (Figure S4). Based on the spectral intensity suppression/cutoff at ∼5.0 eV, an RCB of 2.8 eV is estimated for the omC4P·$[B_{10}H_{10}]^{2-}$ complex. It is worth noting that the RCB of the host–guest complex is expected to be smaller compared to that of the isolated dianion,[68] and the intrinsic RCB of the $[B_{10}H_{10}]^{2-}$ dianion should be larger, given the 3 eV RCB for the analogous $[B_{12}H_{12}]^{2-}$ dianion.[25]

The NIPE spectrum of $[B_{10}H_{10}]^{2-}$ obtained via the above deconvolution scheme is hereby compared to the only measured spectrum in the *closo*-borate $[B_nH_n]^{2-}$ family, i.e., $[B_{12}H_{12}]^{2-}$ (Figure 3).[25,41] Note that the apparent VDE of 1.58 eV is the value affected by the stabilization of omC4P and is thus not a true VDE of $[B_{10}H_{10}]^{2-}$, which is calculated to be negative (Table 1). The more evenly spaced spectral pattern of $[B_{10}H_{10}]^{2-}$ is quite different from that of $[B_{12}H_{12}]^{2-}$, which exhibits one broad band with multiple closely positioned peaks spanning from 0.7 to 3.0 eV, a clear band gap, and followed by another band at 4.2 eV. The clear distinction between these two spectra reflects a very different electronic structure of $[B_{10}H_{10}]^{2-}$ vs $[B_{12}H_{12}]^{2-}$. The I_h symmetry of $[B_{12}H_{12}]^{2-}$ affords a 4-fold degenerate HOMO, a 5-fold degenerate HOMO−1, and a triply degenerate HOMO−2 in the experimental photon energy range (Figure 3d). In contrast, the less symmetric D_{4d} $[B_{10}H_{10}]^{2-}$ is predicted to hold more than 10 states in the same range, resulting in a more complex spectral pattern. These symmetry-induced spectral pattern variations between n = 10 and n = 12 for $[B_nH_n]^{2-}$ were also observed in their halogenated analogs.[18] Based on the charges from electrostatic potentials using a grid-based method (CHELPG)[65] analysis, H atoms in $[B_{10}H_{10}]^{2-}$ carry the majority of negative charges despite the HOMO being dominated by boron atomic orbitals (Figure 2). Moreover,

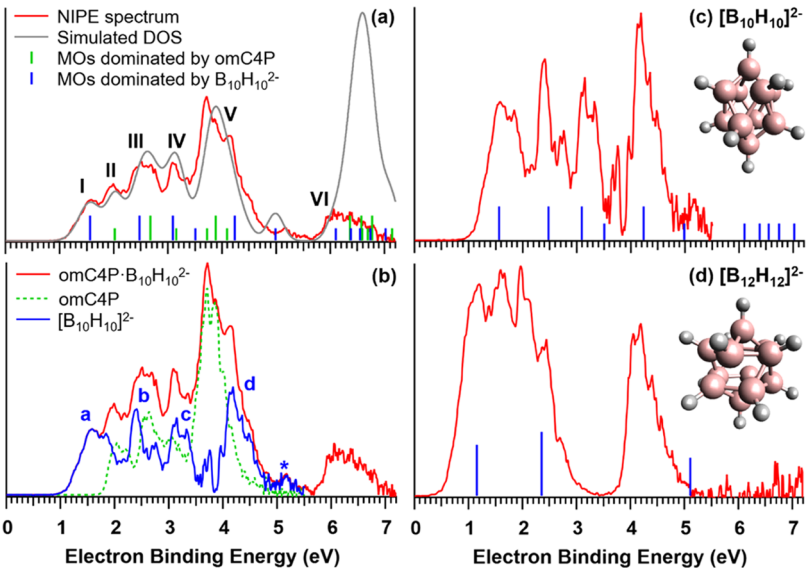

Figure 3. NIPE (red trace) and simulated DOS (gray trace) spectra based on computed M06-2X-D3 MOs of the omC4P·$[B_{10}H_{10}]^{2-}$ complex (green and blue sticks for those dominated by omC4P and $[B_{10}H_{10}]^{2-}$, respectively) (a), deconvolution into contributions from omC4P (green dotted line) and $[B_{10}H_{10}]^{2-}$ (blue trace) with EBE up to 5.5 eV (b), and comparison between the deconvoluted spectrum of $[B_{10}H_{10}]^{2-}$ (c) and previously measured NIPE spectrum of $[B_{12}H_{12}]^{2-}$ (d) and to their computed high-lying MO levels represented in blue sticks. The EBE in part (c) does not reflect the true EBE of $[B_{10}H_{10}]^{2-}$ which could not be experimentally measured. The MOs of $[B_{10}H_{10}]^{2-}$ were calculated with M06-2X-D3, while those of $[B_{12}H_{12}]^{2-}$ were adapted from previous HF calculations, with the length of each stick representing the corresponding MO degeneracy. The spectrum and MOs of $[B_{12}H_{12}]^{2-}$ were adapted with permission from ref 25. Copyright 2024 AIP Publishing.

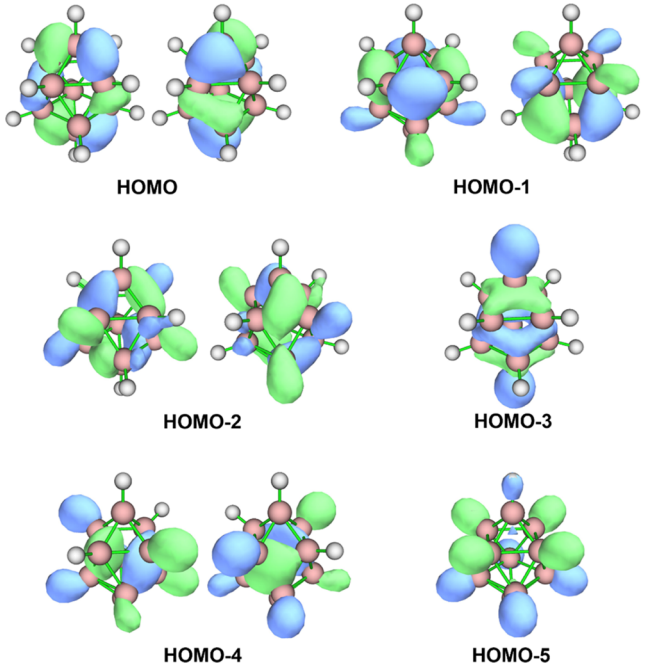

Figure 4. Rendered frontier molecular orbitals (MOs, isovalue = 0.05) of the $[B_{10}H_{10}]^{2-}$ dianion calculated at the M06-2X-D3/maug-cc-pVTZ level of theory.

the reduced symmetry in $[B_{10}H_{10}]^{2-}$ also leads to two different types of B−H environments, under which the equatorial B atoms hold slightly positive charges (0.10e − 0.12e), whereas the two axial B possess negative charges (−0.13e − −0.14e) (Figure 2). Accordingly, the charges on the axial H atoms are less negative (−0.22e) compared to those on the equatorial positions (−0.27e − −0.28e). These nonuniform charge distributions among ten hydridic hydrogens should impact their interactions with surrounding solvent molecules or ligands.

4. CONCLUSIONS

In summary, we have successfully generated omC4P·$[B_{10}H_{10}]^{2-}$ host−guest complexes in the gas phase that contain intact $[B_{10}H_{10}]^{2-}$ dianions, an important species in boron chemistry yet being elusive in the gas phase, by capturing it with an omC4P host molecule. With the previously recorded NIPE spectrum of omC4P·F^- as a reference for the host molecule,[48] a deconvoluted $[B_{10}H_{10}]^{2-}$ spectrum is derived by subtracting the omC4P contribution from the overall spectrum, thus providing spectroscopic information on the electronic structure of $[B_{10}H_{10}]^{2-}$ for the first time. The electronic stabilization afforded by one omC4P molecule is estimated to be 1.75 eV for $[B_{10}H_{10}]^{2-}$, 0.5 eV larger than that for $[B_{12}H_{12}]^{2-}$. The deconvoluted $[B_{10}H_{10}]^{2-}$ spectrum is in good agreement with the simulated DOS spectrum based on the shifted high-lying occupied MO energy pattern. Subsequently, the charge and bonding properties of the $[B_{10}H_{10}]^{2-}$ dianion are investigated, revealing two types of B−H bonds with nonuniform charge distributions on the ligand hydrogens, which may impact its interaction with surrounding solvent molecules. This study also demonstrates that binding with an organic host molecule is an effective means to investigate electronic structures of unstable multiply charged anions.

■ ASSOCIATED CONTENT

Supporting Information

Comparisons in geometric parameters of isolated $[B_{10}H_{10}]^{2-}$ and those of $[B_{10}H_{10}]^{2-}$ within the omC4P complex (Table S1), NIPE spectrum of $[KB_{12}H_{12}]^-$ for comparison (Figure S1), comparisons of NIPE spectra

and computed MO energies of omC4P·$[B_{12}X_{12}]^{2-}$ complexes (Figure S2), deconvolutions of NIPE spectra of omC4P·SO_4^{2-} complexes (Figure S3), and the comparison between deconvoluted $[B_{10}H_{10}]^{2-}$ spectrum and simulated DOS, and two sets of computed MOs (Figure S4) (DOCX)

AUTHOR INFORMATION

Corresponding Author

Xue-Bin Wang − *Physical Sciences Division, Pacific Northwest National Laboratory, Richland, Washington 99352, United States;* orcid.org/0000-0001-8326-1780; Email: xuebin.wang@pnnl.gov

Authors

Wenjin Cao − *Physical Sciences Division, Pacific Northwest National Laboratory, Richland, Washington 99352, United States;* orcid.org/0000-0002-2852-4047

Jonas Warneke − *Wilhelm-Ostwald-Institute for Physical and Theoretical Chemistry, Leipzig University, Leipzig 04103, Germany; Leibniz Institute of Surface Engineering (IOM), Leipzig 04318, Germany;* orcid.org/0000-0002-3233-7412

Notes

The authors declare no competing financial interest.

ACKNOWLEDGMENTS

This work was supported by the U.S. Department of Energy (DOE), Office of Science, Office of Basic Energy Sciences, Division of Chemical Sciences, Geosciences, and Biosciences, Condensed Phase, and Interfacial Molecular Science program, FWP 16248. JW is grateful to a Freigeist Fellowship of the Volkswagen Foundation.

REFERENCES

(1) Lipscomb, W. N. The Boranes and Their Relatives. *Science* **1977**, *196*, 1047−1055.

(2) Pitochelli, A. R.; Hawthorne, F. M. The Isolation of the Icosahedral $B_{12}H_{12}^{2-}$ Ion. *J. Am. Chem. Soc.* **1960**, *82*, 3228−3229.

(3) Aihara, J. Three-Dimensional Aromaticity of Polyhedral Boranes. *J. Am. Chem. Soc.* **1978**, *100*, 3339−3342.

(4) Otsuka, M.; Takita, R.; Kanazawa, J.; Miyamoto, K.; Muranaka, A.; Uchiyama, M. Conjugation between σ- and π-Aromaticity in 1-C-Arylated Monocarba-closo-dodecaborate Anions. *J. Am. Chem. Soc.* **2015**, *137*, 15082−15085.

(5) Axtell, J. C.; Saleh, L. M. A.; Qian, E. A.; Wixtrom, A. I.; Spokoyny, A. M. Synthesis and Applications of Perfunctionalized Boron Clusters. *Inorg. Chem.* **2018**, *57*, 2333−2350.

(6) Poater, J.; Escayola, S.; Poater, A.; Teixidor, F.; Ottosson, H.; Viñas, C.; Solà, M. Single—Not Double—3D-Aromaticity in an Oxidized Closo Icosahedral Dodecaiodo-Dodecaborate Cluster. *J. Am. Chem. Soc.* **2023**, *145*, 22527−22538.

(7) Warneke, J. Gas-Phase Ion Chemistry of $[B_{12}X_{12}]^{2-}$ (X = F, Cl, Br, I, CN). A Brief Review of Twelve Years of Researching Twelve−Vertexed Dianions and Their Fragments. *Int. J. Mass spectrom.* **2024**, *496*, No. 117169.

(8) Hawthorne, M. F. The Role of Chemistry in the Development of Boron Neutron Capture Therapy of Cancer. *Angew. Chem., Int. Ed.* **1993**, *32*, 950−984.

(9) Hosmane, N. S. *Boron Science: New Technologies and Applications*; CRC Press, 2011.

(10) Giri, S.; Behera, S.; Jena, P. Superhalogens as Building Blocks of Halogen-Free Electrolytes in Lithium-Ion Batteries. *Angew. Chem., Int. Ed.* **2014**, *53*, 13916−13919.

(11) Tutusaus, O.; Mohtadi, R.; Arthur, T. S.; Mizuno, F.; Nelson, E. G.; Sevryugina, Y. V. An Efficient Halogen-Free Electrolyte for Use in Rechargeable Magnesium Batteries. *Angew. Chem., Int. Ed.* **2015**, *54*, 7900−7904.

(12) Tang, W. S.; Unemoto, A.; Zhou, W.; Stavila, V.; Matsuo, M.; Wu, H.; Orimo, S.-i.; Udovic, T. J. Unparalleled lithium and sodium superionic conduction in solid electrolytes with large monovalent cage-like anions. *Energy Environ. Sci.* **2015**, *8*, 3637−3645.

(13) Zhao, H.; Zhou, J.; Jena, P. Stability of $B_{12}(CN)_{12}^{2-}$: Implications for Lithium and Magnesium Ion Batteries. *Angew. Chem., Int. Ed.* **2016**, *55*, 3704−3708.

(14) Payandeh, S.; Asakura, R.; Avramidou, P.; Rentsch, D.; Łodziana, Z.; Černý, R.; Remhof, A.; Battaglia, C. Nido-Borate/Closo-Borate Mixed-Anion Electrolytes for All-Solid-State Batteries. *Chem. Mater.* **2020**, *32*, 1101−1110.

(15) Ready, A. D.; Irshad, A.; Kallistova, A.; Carrillo, M.; Gembicky, M.; Seshadri, R.; Narayan, S.; Spokoyny, A. M. Electrochemical Cycling of Redox-Active Boron Cluster-Based Materials in the Solid State. *J. Am. Chem. Soc.* **2023**, *145*, 14345−14353.

(16) Sivaev, I. B.; Prikaznov, A. V.; Naoufal, D. Fifty years of the closo-decaborate anion chemistry. *Collect. Czech. Chem. Commun.* **2010**, *75*, 1149−1199.

(17) Zhong, M.; Zhou, J.; Fang, H.; Jena, P. Role of Ligands in the Stability of B_nX_n and $CB_{n-1}X_n$ (n = 5−10; X = H, F, CN) and Their Potential as Building Blocks of Electrolytes in Lithium Ion Batteries. *Phys. Chem. Chem. Phys.* **2017**, *19*, 17937−17943.

(18) Warneke, J.; Konieczka, S. Z.; Hou, G.-L.; Aprà, E.; Kerpen, C.; Keppner, F.; Schäfer, T. C.; Deckert, M.; Yang, Z.; Bylaska, E. J.; et al. Properties of Perhalogenated {closo-B_{10}} and {closo-B_{11}} Multiply Charged Anions and a Critical Comparison with {closo-B_{12}} in the Gas and the Condensed Phase. *Phys. Chem. Chem. Phys.* **2019**, *21*, 5903−5915.

(19) Rohdenburg, M.; Yang, Z.; Su, P.; Bernhardt, E.; Yuan, Q.; Apra, E.; Grabowsky, S.; Laskin, J.; Jenne, C.; Wang, X.-B.; et al. Properties of Gaseous closo-$[B_6X_6]^{2-}$ Dianions (X = Cl, Br, I). *Phys. Chem. Chem. Phys.* **2020**, *22*, 17713−17724.

(20) Kawa, S.; Knorke, H.; Jin, J.; Rohdenburg, M.; Asmis, K. R.; Tonner-Zech, R.; Bernhardt, E.; Jenne, C.; Finze, M.; Warneke, J. Binding Properties of Small Electrophilic Anions $[B_6X_5]^-$ and $[B_{10}X_9]^-$ (X = Cl, Br, I): Activation of Small Molecules Based on π-Backbonding. *Chem. - Eur. J.* **2023**, *29*, No. e202302247, DOI: 10.1002/chem.202302247.

(21) Soloway, A. H.; Tjarks, W.; Barnum, B. A.; Rong, F.-G.; Barth, R. F.; Codogni, I. M.; Wilson, J. G. The Chemistry of Neutron Capture Therapy. *Chem. Rev.* **1998**, *98*, 1515−1562.

(22) Wilbur, D. S.; Chyan, M.-K.; Hamlin, D. K.; Perry, M. A. Reagents for Astatination of Biomolecules. 3. Comparison of closo-Decaborate(2-) and closo-Dodecaborate(2-) Moieties as Reactive Groups for Labeling with Astatine-211. *Bioconjugate Chem.* **2009**, *20*, 591−602.

(23) Yuan, Q.; Cao, W.; Wang, X.-B. Cryogenic and Temperature-Dependent Photoelectron Spectroscopy of Metal Complexes. *Int. Rev. Phys. Chem.* **2020**, *39*, 83−108.

(24) Warneke, J.; Wang, X.-B. Measuring Electronic Structure of Multiply Charged Anions to Understand Their Chemistry: A Case Study on Gaseous Polyhedral closo-Borate Dianions. *J. Phys. Chem. A* **2021**, *125*, 6653−6661.

(25) Aprà, E.; Warneke, J.; Xantheas, S. S.; Wang, X.-B. A Benchmark Photoelectron Spectroscopic and Theoretical Study of the Electronic Stability of $[B_{12}H_{12}]^{2-}$. *J. Chem. Phys.* **2019**, *150*, No. 164306, DOI: 10.1063/1.5089510.

(26) Warneke, J.; Hou, G.-L.; Aprà, E.; Jenne, C.; Yang, Z.; Qin, Z.; Kowalski, K.; Wang, X.-B.; Xantheas, S. S. Electronic Structure and Stability of $[B_{12}X_{12}]^{2-}$ (X = F−At): A Combined Photoelectron Spectroscopic and Theoretical Study. *J. Am. Chem. Soc.* **2017**, *139*, 14749−14756.

(27) Mayer, M.; van Lessen, V.; Rohdenburg, M.; Hou, G.-L.; Yang, Z.; Exner, R. M.; Aprà, E.; Azov, V. A.; Grabowsky, S.; Xantheas, S. S.; et al. Rational Design of an Argon-Binding Superelectrophilic Anion. *Proc. Natl. Acad. Sci. U.S.A.* **2019**, *116*, 8167−8172.
(28) Asmis, K. R.; Beele, B. B.; Jenne, C.; Kawa, S.; Knorke, H.; Nierstenhöfer, M. C.; Wang, X.-B.; Warneke, J.; Warneke, Z.; Yuan, Q. Synthesis, Electronic Properties and Reactivity of $[B_{12}X_{11}(NO_2)]^{2-}$ (X = F−I) Dianions. *Chem. - Eur. J.* **2020**, *26*, 14594−14601, DOI: 10.1002/chem.202003537.
(29) Scheller, M. K.; Compton, R. N.; Cederbaum, L. S. Gas-Phase Multiply Charged Anions. *Science* **1995**, *270*, 1160−1166.
(30) Boxford, W. E.; Dessent, C. E. H. Probing the Intrinsic Features and Environmental Stabilization of Multiply Charged Anions. *Phys. Chem. Chem. Phys.* **2006**, *8*, 5151−5165.
(31) Zint, N.; Dreuw, A.; Cederbaum, L. S. Gas-Phase Stability of Derivatives of the closo-Hexaborate Dianion $B_6H_6^{2-}$. *J. Am. Chem. Soc.* **2002**, *124*, 4910−4917.
(32) McKee, M. L.; Wang, Z.-X.; Schleyer, P. v. R. Ab Initio Study of the Hypercloso Boron Hydrides B_nH_n and $B_nH_n^-$. Exceptional Stability of Neutral $B_{13}H_{13}$. *J. Am. Chem. Soc.* **2000**, *122*, 4781−4793.
(33) Lee, T. B.; McKee, M. L. Redox Energetics of Hypercloso Boron Hydrides B_nH_n (n = 6−13) and $B_{12}X_{12}$ (X = F, Cl, OH, and CH_3). *Inorg. Chem.* **2012**, *51*, 4205−4214.
(34) Tahaoğlu, D.; Alkan, F.; Durandurdu, M. Theoretical Investigation of Substituent Effects on the Relative Stabilities and Electronic Structure of $[B_nX_n]^{2-}$ Clusters. *J. Mol. Model.* **2021**, *27*, No. 365, DOI: 10.1007/s00894-021-04980-1.
(35) Hawthorne, M. F.; Pilling, R. L.; Knoth, W. H. Bis-(triethylammonium) Decahydrodecaborate(2−). *Inorg. Synth.* **1967**, *9*, 16−19.
(36) Mahfouz, N.; Ghaida, F. A.; El Hajj, Z.; Diab, M.; Floquet, S.; Mehdi, A.; Naoufal, D. Recent Achievements on Functionalization within closo-Decahydrodecaborate $[B_{10}H_{10}]^{2-}$ Clusters. *ChemistrySelect* **2022**, *7*, No. e202200770, DOI: 10.1002/slct.202200770.
(37) Lu, Z.; Qiu, P.; Kang, J.-X.; Chen, X.; Zhang, G.; Zhang, Y.; Chen, X. Potassium Decahydrido-closo-Decaborane Urea Complex as a Potential Solid-State Electrolyte for Potassium Metal Batteries. *ACS Appl. Mater. Interfaces* **2024**, *16*, 10070−10077.
(38) Wang, X.-B. Cluster Model Studies of Anion and Molecular Specificities via Electrospray Ionization Photoelectron Spectroscopy. *J. Phys. Chem. A* **2017**, *121*, 1389−1401.
(39) Wang, X.-B.; Nicholas, J. B.; Wang, L.-S. Electronic Instability of Isolated SO_4^{2-} and its Solvation Stabilization. *J. Chem. Phys.* **2000**, *113*, 10837−10840.
(40) Jiang, Y.; Yuan, Q.; Cao, W.; Hu, Z.; Yang, Y.; Zhong, C.; Yang, T.; Sun, H.; Wang, X.-B.; Sun, Z. Unraveling Hydridic-to-Protonic Dihydrogen Bond Predominance in Monohydrated Dodecaborate Clusters. *Chem. Sci.* **2022**, *13*, 9855−9860.
(41) Jiang, Y.; Cai, Z.; Yuan, Q.; Cao, W.; Hu, Z.; Sun, H.; Wang, X.-B.; Sun, Z. Highly Structured Water Networks in Microhydrated Dodecaborate Clusters. *J. Phys. Chem. Lett.* **2022**, *13*, 11787−11794.
(42) Assaf, K. I.; Ural, M. S.; Pan, F.; Georgiev, T.; Simova, S.; Rissanen, K.; Gabel, D.; Nau, W. M. Water Structure Recovery in Chaotropic Anion Recognition: High-Affinity Binding of Dodecaborate Clusters to γ-Cyclodextrin. *Angew. Chem., Int. Ed.* **2015**, *54*, 6852−6856.
(43) Warneke, J.; Jenne, C.; Bernarding, J.; Azov, V. A.; Plaumann, M. Evidence for an Intrinsic Binding Force between Dodecaborate Dianions and Receptors with Hydrophobic Binding Pockets. *Chem. Commun.* **2016**, *52*, 6300−6303.
(44) Diab, M.; Floquet, S.; Haouas, M.; Abramov, P. A.; López, X.; Landy, D.; Damond, A.; Falaise, C.; Guérineau, V.; Touboul, D.; et al. Encapsulation of Chaotropic closo-Decahydrodecaborate Clusters Within Cyclodextrins: Synthesis, Solution Studies, and DFT Calculations. *Eur. J. Inorg. Chem.* **2019**, *2019*, 3373−3382.
(45) Li, Z.; Jiang, Y.; Yuan, Q.; Warneke, J.; Hu, Z.; Yang, Y.; Sun, H.; Sun, Z.; Wang, X.-B. Photoelectron Spectroscopy and Computational Investigations of the Electronic Structures and Noncovalent Interactions of Cyclodextrin-closo-Dodecaborate Anion Complexes χ-CD·$B_{12}X_{12}^{2-}$ (χ = α, β, γ; X = H, F). *Phys. Chem. Chem. Phys.* **2020**, *22*, 7193−7200.
(46) Jiang, Y.; Yuan, Q.; Cao, W.; Rohdenburg, M.; Nierstenhöfer, M. C.; Li, Z.; Yang, Y.; Zhong, C.; Jenne, C.; Warneke, J.; et al. Gaseous Cyclodextrin-closo-Dodecaborate Complexes χCD·$B_{12}X_{12}^{2-}$ (χ = α, β, and γ; X = F, Cl, Br, and I): Electronic Structures and Intramolecular Interactions. *Phys. Chem. Chem. Phys.* **2021**, *23*, 13447−13457.
(47) El Hajj, Z.; Calancea, S.; Haouas, M.; Landy, D.; Naoufal, D.; Floquet, S. Playing with the Chaotropic Effect to Improve the Encapsulation of Decaborate Clusters within Cyclodextrins. *J. Cluster Sci.* **2024**, *35*, 253−263.
(48) Cao, W.; Wang, X. Organic Molecules Mimic Alkali Metals Enabling Spontaneous Harpoon Reactions with Halogens. *Chem. - Eur. J.* **2024**, *30*, No. e202400038, DOI: 10.1002/chem.202400038.
(49) Gale, P. A.; Sessler, J. L.; Král, V.; Lynch, V. Calix[4]pyrroles: Old Yet New Anion-Binding Agents. *J. Am. Chem. Soc.* **1996**, *118*, 5140−5141.
(50) Terry, L. M.; Foreman, M. M.; Rasmussen, A. P.; McCoy, A. B.; Weber, J. M. Probing Ion-Receptor Interactions in Halide Complexes of Octamethyl Calix [4] Pyrrole *ChemRxiv* 2023 DOI: 10.26434/chemrxiv-2023-59dcd (accessed April 14, 2024).
(51) Hanstorp, D.; Gustafsson, M. Determination of the Electron Affinity of Iodine. *J. Phys. B: At., Mol. Opt. Phys.* **1992**, *25*, 1773.
(52) Wang, X.-B.; Wang, L.-S. Photodetachment of Free Hexahalogenometallate Doubly Charged Anions in the Gas Phase: $[ML_6]^{2-}$, (M = Re, Os, Ir, Pt; L = Cl and Br). *J. Chem. Phys.* **1999**, *111*, 4497−4509.
(53) Zhao, Y.; Truhlar, D. G. The M06 Suite of Density Functionals for Main Group Thermochemistry, Thermochemical Kinetics, Noncovalent Interactions, Excited States, and Transition Elements: Two New Functionals and Systematic Testing of Four M06-Class Functionals and 12 Other Functionals. *Theor. Chem. Acc.* **2008**, *120*, 215−241.
(54) Grimme, S.; Antony, J.; Ehrlich, S.; Krieg, H. A Consistent and Accurate ab Initio Parametrization of Density Functional Dispersion Correction (DFT-D) for the 94 Elements H-Pu. *J. Chem. Phys.* **2010**, *132*, No. 154104, DOI: 10.1063/1.3382344.
(55) Weigend, F.; Ahlrichs, R. Balanced Basis Sets of Split Valence, Triple Zeta Valence and Quadruple Zeta Valence Quality for H to Rn: Design and Assessment of Accuracy. *Phys. Chem. Chem. Phys.* **2005**, *7*, 3297−3305.
(56) Dunning, T. H., Jr Gaussian Basis Sets for Use in Correlated Molecular Calculations. I. The Atoms Boron Through Neon and Hydrogen. *J. Chem. Phys.* **1989**, *90*, 1007−1023.
(57) Papajak, E.; Zheng, J.; Xu, X.; Leverentz, H. R.; Truhlar, D. G. Perspectives on Basis Sets Beautiful: Seasonal Plantings of Diffuse Basis Functions. *J. Chem. Theory Comput.* **2011**, *7*, 3027−3034.
(58) Peterson, K. A.; Shepler, B. C.; Figgen, D.; Stoll, H. On the Spectroscopic and Thermochemical Properties of ClO, BrO, IO, and Their Anions. *J. Phys. Chem. A* **2006**, *110*, 13877−13883.
(59) Riplinger, C.; Pinski, P.; Becker, U.; Valeev, E. F.; Neese, F. Sparse Maps—A Systematic Infrastructure for Reduced-Scaling Electronic Structure Methods. II. Linear Scaling Domain Based Pair Natural Orbital Coupled Cluster Theory. *J. Chem. Phys.* **2016**, *144*, No. 024109, DOI: 10.1063/1.4939030.
(60) Liu, B.; McLean, A. D. Accurate Calculation of the Attractive Interaction of Two Ground State Helium Atoms. *J. Chem. Phys.* **1973**, *59*, 4557−4558.
(61) Boys, S. F.; Bernardi, F. The Calculation of Small Molecular Interactions by the Differences of Separate Total Energies. Some Procedures with Reduced Errors. *Mol. Phys.* **1970**, *19*, 553−566.
(62) Weigend, F. A fully direct RI-HF algorithm: Implementation, optimized auxiliary basis sets, demonstration of accuracy and efficiency. *Phys. Chem. Chem. Phys.* **2002**, *4*, 4285−4291.
(63) Neese, F.; Wennmohs, F.; Becker, U.; Riplinger, C. The ORCA Quantum Chemistry Program Package. *J. Chem. Phys.* **2020**, *152*, No. 224108, DOI: 10.1063/5.0004608.

(64) Neese, F. Software update: The ORCA program system—Version 5.0. *Wiley Interdiscip. Rev.: Comput. Mol. Sci.* **2022**, *12*, No. e1606, DOI: 10.1002/wcms.1606.
(65) Chirlian, L. E.; Francl, M. M. Atomic Charges Derived from Electrostatic Potentials: A Detailed Study. *J. Comput. Chem.* **1987**, *8*, 894−905.
(66) Lu, T.; Chen, F. Multiwfn: A Multifunctional Wavefunction Analyzer. *J. Comput. Chem.* **2012**, *33*, 580−592.
(67) Sen, A.; Matthews, E. M.; Hou, G.-L.; Wang, X.-B.; Dessent, C. E. H. Photoelectron Spectroscopy of Hexachloroplatinate-Nucleobase Complexes: Nucleobase Excited State Decay Observed via Delayed Electron Emission. *J. Chem. Phys.* **2015**, *143*, No. 184307, DOI: 10.1063/1.4935171.
(68) Jiang, Y.; Hu, Z.; Yang, Y.; Peng, P.; Zhong, C.; Sun, H.; Sun, Z.; Wang, X.-B. Beyond Duality: Rationalizing Repulsive Coulomb Barriers in Host−Guest Cyclodextrin−Dodecaborate Complexes. *J. Phys. Chem. Lett.* **2023**, *14*, 6736−6742.